Supplement of Atmos. Chem. Phys., 26, 5679–5696, 2026
https://doi.org/10.5194/acp-26-5679-2026-supplement

Atmospheric Chemistry and Physics
Open Access
EGU

Supplement of

The radiative forcing of $PM_{2.5}$ heavy pollution, its influencing factors and importance to precipitation during 2014–2023 in the Bohai Rim, China

Jun Zhu et al.

Correspondence to: Xu Yue (yuexu@nuist.edu.cn) and Huizheng Che (chehz@cma.ac.cn)

Supplementary file

Table S1. Site information of 11 ground-observed stations

Regions	Station name	Station Abbr.	Longitude(°E)	latitude(°N)
West of the Bohai Sea (BLT)	Beijing	BJ	116.398	40.046
	Langfang	LF	116.724	39.546
	Tianjin	TJ	117.324	39.100
North of the Bohai Sea (NB)	Tangshan	TS	118.183	39.645
	Qinghuangdao	QHD	119.607	39.936
	Huludao	HLD	120.865	40.738
	Dalian	DL	121.628	38.950
South of the Bohai Sea (SB)	Cangzhou	CZ	116.872	38.316
	Dongying	DY	118.654	37.431
	Yantai	YT	121.406	37.488
	Weihai	WH	122.093	37.490

Table S2. The essential statistical metrics of the evaluation of Random Forest training models.

Statistical metrics	RF surface clear	RF surface all	RF TOA clear	RF TOA all	RF Atmos clear	RF Atmos all	Total pre
R^2	0.6721	0.6722	0.6852	0.6512	0.6557	0.6742	0.5728
RMSE	0.5697	0.5697	0.5562	0.5881	0.5837	0.5683	0.6454
MAE	0.4277	0.4291	0.3921	0.4381	0.4442	0.4416	0.2410

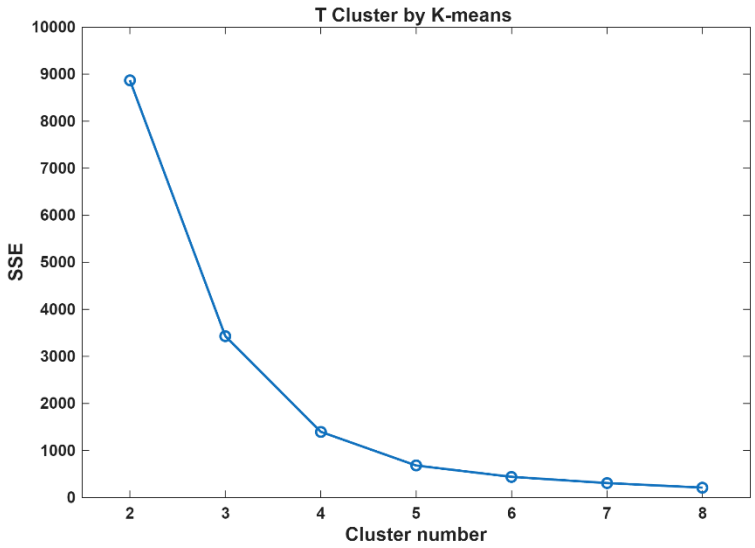

Figure S1. The Sum of Squared Errors (SSE) of k-means clustering of T using the cluster numbers from 2 to 8. The number 5 is nearing the "elbow point" where adding more clusters yields diminishing returns in reducing within-cluster variance.

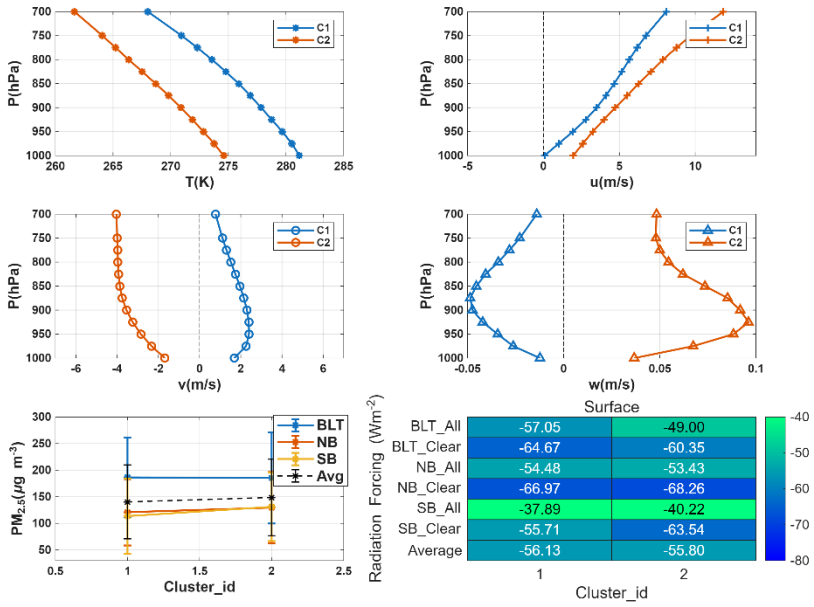

Figure S2. The results of clustering of combined T and winds by the k-means algorithm using the elbow method to determine the number of clusters of 2 (this clustering of 2 is distinct for temperature and winds, but failed to capture the temperature inversion layers).

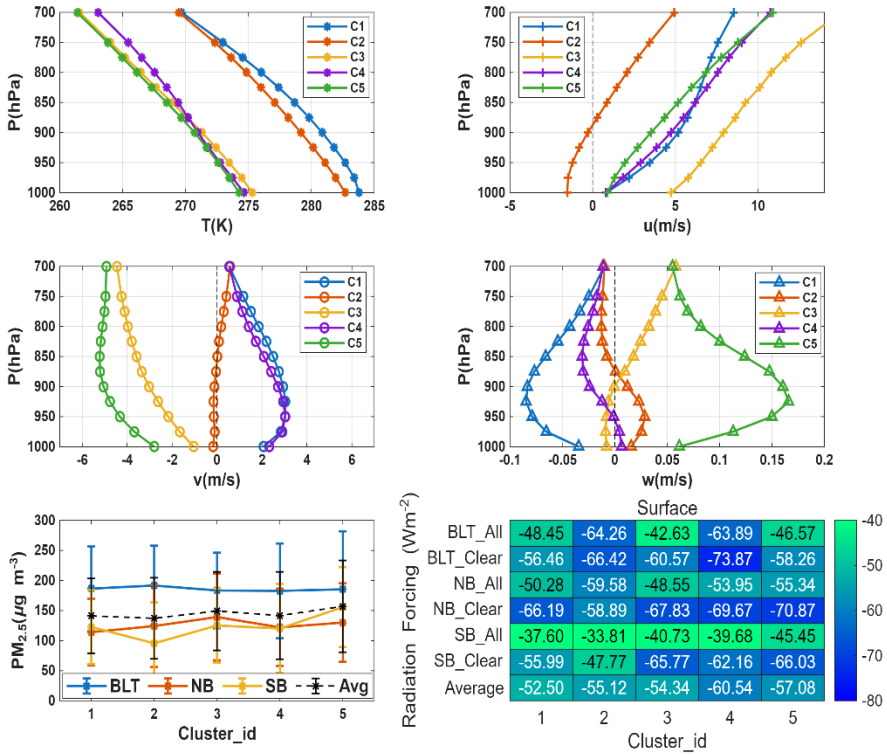

Figure S3. The results of clustering of combined T and winds by the k-means algorithm using the same number of clusters in the manuscript of 5 (this clustering of 5 also failed to capture the temperature inversion layers).

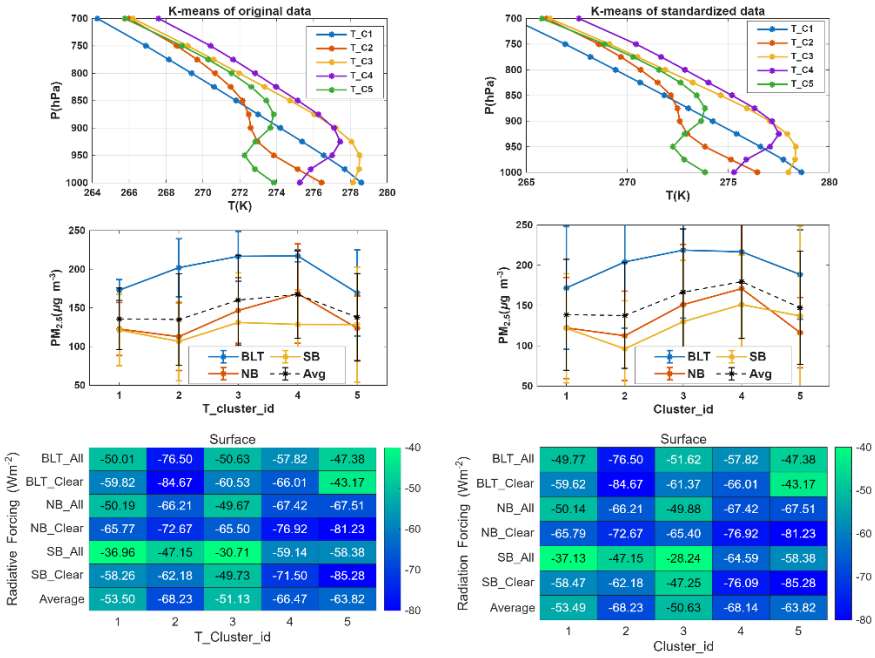

Figure S4. The comparison of k-means clustering by using original data and standardized data (Z-score of T).

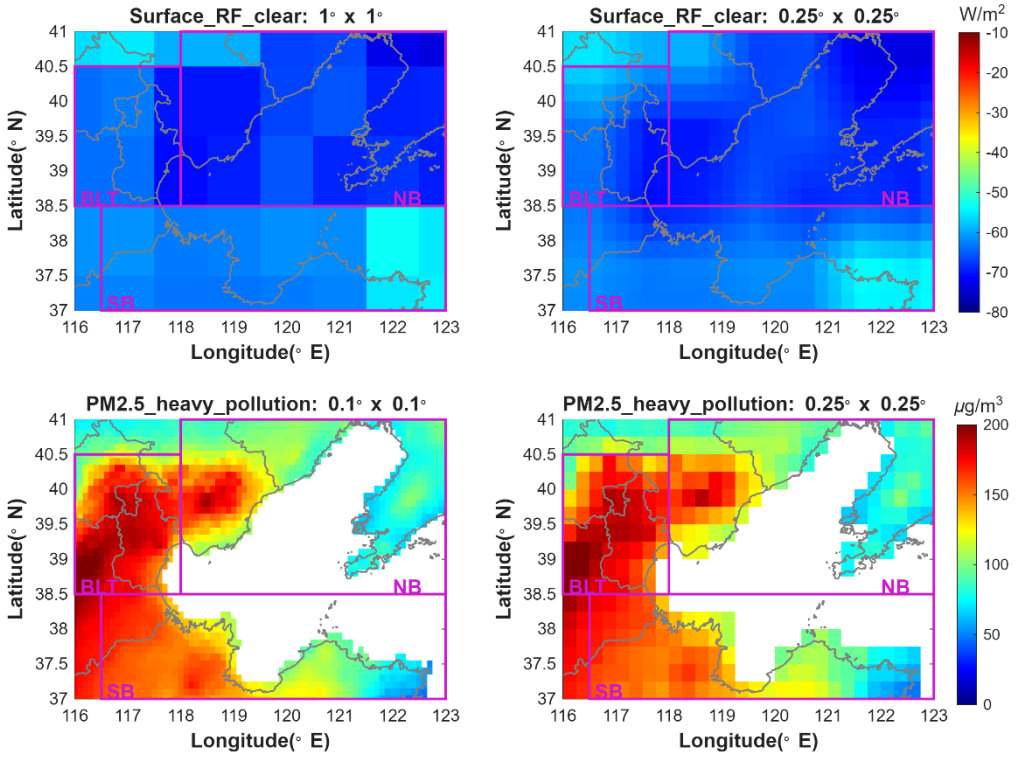

Figure S5. The comparison between the original data (first column) and the interpolated data (second column) in the study area. The first row is the radiative forcing (RF) from CERES at the surface in clear sky, and the second row is the interpolation for the $PM_{2.5}$ from TAP. The purple rectangle indicates the three regions.

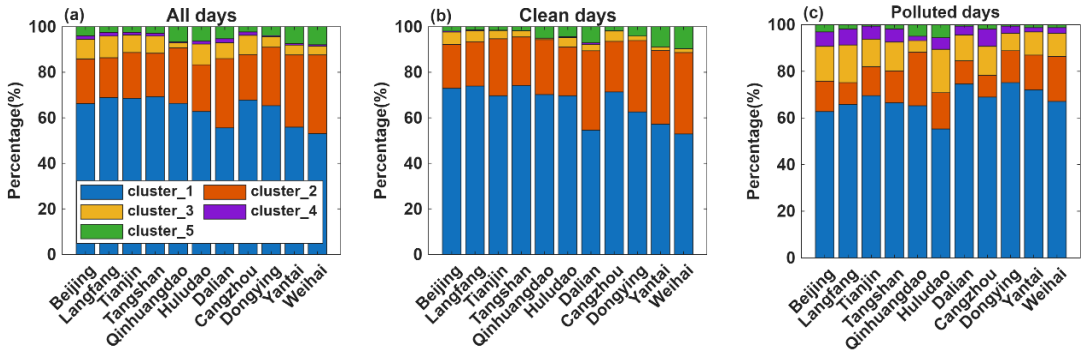

Figure S6. Proportions of different temperature profile types (C1: decreasing, C2: decreasing with isotherms, C3: low-altitude inversion, C4: mid-altitude inversion, and C5: upper-altitude inversion) on all days (a), regional clean days (b), and regional heavy polluted days (c) at each station during autumn and winter 2014-2023.

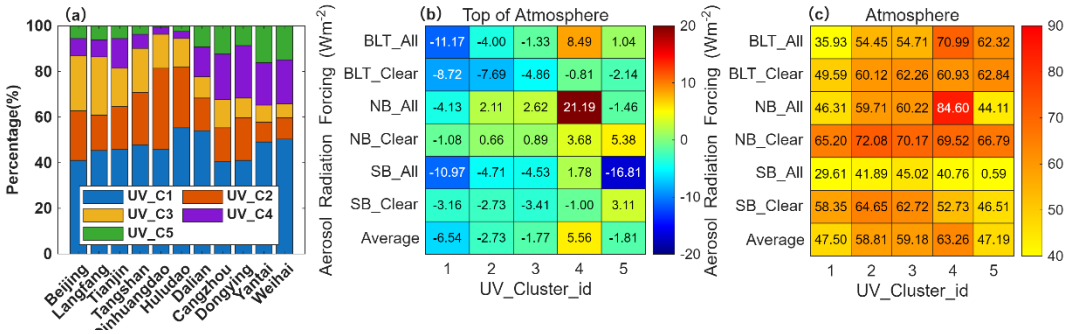

Figure S7. The percentage statistics at the 11 stations (a) and radiative forcing in the three regions in clear- and all-sky at the top of the atmosphere (b), and in the atmosphere (c) at the five horizontal wind clusters.

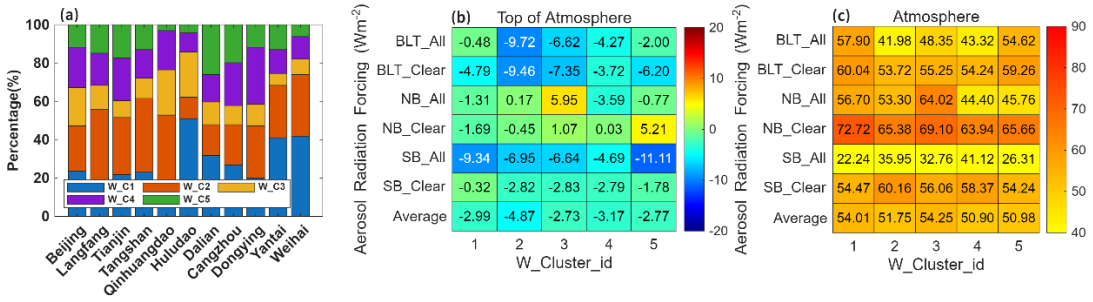

Figure S8. The percentage statistics at the 11 stations (a) and radiative forcing in the three regions in clear- and all-sky at the top of the atmosphere (b), and in the atmosphere (c) at the five vertical wind clusters.